

Impact of large-mass constraints on the properties of neutron stars

Christian Ecker¹★ and Luciano Rezzolla^{1,2,3}

¹*Institut für Theoretische Physik, Goethe Universität, Max-von-Laue-Str. 1, 60438 Frankfurt am Main, Germany*

²*School of Mathematics, Trinity College, Dublin 2, Ireland*

³*Frankfurt Institute for Advanced Studies, Ruth-Moufang-Str. 1, 60438 Frankfurt am Main, Germany*

Accepted XXX. Received YYY; in original form ZZZ

ABSTRACT

The maximum mass of a nonrotating neutron star, M_{TOV} , plays a very important role in deciphering the structure and composition of neutron stars and in revealing the equation of state (EOS) of nuclear matter. Although with a large-error bar, the recent mass estimate for the black-widow binary pulsar PSR J0952-0607, i.e., $M = 2.35 \pm 0.17 M_{\odot}$, provides the strongest lower bound on M_{TOV} and suggests that neutron stars with very large masses can in principle be observed. Adopting an agnostic modelling of the EOS, we study the impact that large masses have on the neutron-star properties. In particular, we show that assuming $M_{\text{TOV}} \gtrsim 2.35 M_{\odot}$ constrains tightly the behaviour of the pressure as a function of the energy density and moves the lower bounds for the stellar radii to values that are significantly larger than those constrained by the NICER measurements, rendering the latter ineffective in constraining the EOS. We also provide updated analytic expressions for the lower bound on the binary tidal deformability in terms of the chirp mass and show how larger bounds on M_{TOV} lead to tighter constraints for this quantity. In addition, we point out a novel quasi-universal relation for the pressure profile inside neutron stars that is only weakly dependent from the EOS and the maximum-mass constraint. Finally, we study how the sound speed and the conformal anomaly are distributed inside neutron stars and show how these quantities depend on the imposed maximum-mass constraints.

Key words: neutron stars – equation of state – sound speed

1 INTRODUCTION

The maximum mass beyond which a static relativistic star collapses to a black hole, M_{TOV} , is determined by the solution of the equilibrium equations for a self-gravitating fluid configuration – the so-called Tolmann-Oppenheimer-Volkoff (TOV) equations – once an equation of state (EOS), that is a relation between the pressure and the energy density $p(e)$, is specified. Given the intimate relation between the EOS and the maximum mass, the knowledge of the latter has always been considered an essential tool to access the former.

Chiral Effective Theory (CET) calculations (Hebeler et al. 2013; Gandolfi et al. 2019; Keller et al. 2021; Drischler et al. 2020) constrain the EOS at baryon densities n below and around nuclear saturation density $n_s = 0.16 \text{ fm}^{-3}$. At densities much higher than those realised inside neutron stars ($n \gg n_s$), matter is in a state of deconfined quarks and gluons and the EOS of Quantum Chromodynamics (QCD) becomes accessible to perturbation theory (Freedman & McLerran 1977; Vuorinen 2003; Gorda et al. 2021a). Between these limits, at densities a few times larger than n_s , such as those realised in neutron-star cores, these methods are not applicable, hence our knowledge about even the most basic neutron-star properties like their mass-radius relation and in particular their maximum mass is incomplete. In this regime the currently available theoretical options are specific-model building (see, e.g., Bastian 2021; Demircik et al. 2021a; Ivanytskyi & Blaschke 2022, for some recent works), and model agnostic EOS-samplings (see, e.g., Greif et al. 2019; An-

nala et al. 2020; Dietrich et al. 2020; Altiparmak et al. 2022, for some recent attempts), for which CET and QCD provide important constraints (Komoltsev & Kurkela 2022; Gorda et al. 2022; Somasundaram et al. 2022).

In addition, a number of EOS independent quasi-universal relations have been identified among various neutron-star properties, either when isolated (see, e.g., Yagi & Yunes 2013) or when in binary systems (see, e.g., Baiotti & Rezzolla 2017). These relations provide a useful tool to break the degeneracy between existing uncertainties in the EOS and differences between General Relativity and alternative theories of gravity. Quasi-universal relations have also been found to describe the critical mass of equilibrium models with varying angular momentum, that is, the maximum mass along the stability line of uniformly rotating configurations. In turn, this relation allows one to tightly constrain the ratio between the maximum mass of uniformly rotating and static stars made of purely nucleonic matter, i.e., $M_{\text{max}} = 1.203^{+0.022}_{-0.022} M_{\text{TOV}}$ (Breu & Rezzolla 2016) and to only slightly larger values when accounting for a phase transition to quark matter (Bozzola et al. 2019; Demircik et al. 2021b).

On the observational side, direct mass measurements of $M \approx 2 M_{\odot}$ (Antoniadis et al. 2013; Cromartie et al. 2019; Fonseca et al. 2021), combined with mass and radius measurements by the NICER experiment (Riley et al. 2019; Miller et al. 2019; Miller et al. 2021; Riley et al. 2021) and with measurements of the binary tidal deformability $\tilde{\Lambda}$ from the binary neutron-star merger GW170817 (The LIGO Scientific Collaboration et al. 2019), have provided until recently the most important benchmarks for the EOS at densities beyond n_s . The direct mass measurement of the heavy companion in the black-widow

★ E-mail: ecker@itp.uni-frankfurt.de (CE)

binary pulsar PSR J0952-0607, namely $M = 2.35 \pm 0.17 M_\odot$ by [Romani et al. \(2022\)](#), significantly exceeds the results of any previous mass measurements. Although reported with a large uncertainty, such a measurement represents currently the most massive known neutron star and provides the strictest lower bound on the maximum neutron-star mass to this date. This *observational* mass measurement, at least in its lower bound, is still compatible with the theoretical predictions made for the maximum mass by a number of groups on the basis of the GW170817 event and the corresponding gamma-ray burst event GRB170817A, namely $M_{\text{TOV}} \lesssim 2.16^{+0.17}_{-0.15} M_\odot$ ([Margalit & Metzger 2017](#); [Rezzolla et al. 2018](#); [Ruiz et al. 2018](#); [Shibata et al. 2019](#)). In addition, recent work taking into account the GW190814 event, has shown that maximum masses in excess of $\approx 2.4 M_\odot$ have problems satisfying the limits on the gravitational mass emitted in gravitational waves or the rest-mass ejected after the merger ([Nathanail et al. 2021](#)).

Obviously, the novel mass constraint provided by PSR J0952-0607, and the future refinements that are expected to reduce the measurement uncertainties, will provide very important input to further sharpen the focus on the properties of neutron stars and, in particular, on some of the most basic features of any EOS. One such quantity is the adiabatic sound speed ([Rezzolla & Zanotti 2013](#))

$$c_s^2 := \left(\frac{\partial p}{\partial e} \right)_s, \quad (1)$$

where p , e , and s are the pressure, energy density and specific entropy, respectively; clearly, the sound speed is bounded by causality and thermodynamic stability to $0 \leq c_s^2 \leq 1$. Because the sound speed provides a direct measure of the stiffness of matter within the star, it represents a very accurate tool to probe the stellar interior and is obviously directly related the maximum mass that any EOS can support. The properties of the sound speed at finite densities have been studied extensively with various approaches in the recent past (see, e.g., [Ecker et al. 2017](#); [McLerran & Reddy 2019](#); [Leonhardt et al. 2020](#); [Margueron et al. 2021](#); [Duarte et al. 2021](#); [Pal et al. 2022](#); [Altiparmak et al. 2022](#); [Brandes et al. 2022](#); [Braun & Schallmo 2022](#); [Ecker & Rezzolla 2022](#), and references therein). There is now widespread consensus that the sound speed is much smaller than the speed of light ($c_s^2 \ll 1$) in low-density matter ($n \lesssim n_s$) and approaches the conformal limit $c_s^2 = 1/3$ from below at large densities ($n \gtrsim 40 n_s$). In between, the sound speed is most likely non-monotonic and reaches a local maximum that exceeds the conformal value $c_s^2 > 1/3$ at densities few times larger than n_s ([Altiparmak et al. 2022](#)). Because this local maximum in the sound speed at densities typically probed by neutron-star interiors was already necessary to explain the previous bounds on the maximum-mass measurements $M \gtrsim 2 M_\odot$ (see the arguments by [Bedaque & Steiner 2015](#); [Hoyos et al. 2016](#); [Moustakidis et al. 2017](#); [Kanakis-Pegios et al. 2020](#)), the recent bound set by PSR J0952-0607 has the direct consequence of moving the maximum to even larger values and lower densities.

Another quantity related to the stellar interior that has been recently attracted considerable interest (see, e.g., [Fujimoto et al. 2022](#); [Marczenko et al. 2022](#)) is the so-called “conformal anomaly”, that is, the normalized trace of the star’s energy-momentum tensor $T^{\mu\nu}$

$$\Delta := \frac{1}{3} \frac{g_{\mu\nu} T^{\mu\nu}}{e} = \frac{1}{3} - \frac{p}{e}, \quad (2)$$

where $g_{\mu\nu}$ is the metric tensor and the second equality in Eq. (2) refers to a perfect fluid and is true for any metric and coordinate system ([Rezzolla & Zanotti 2013](#)). Requiring that the conformal anomaly satisfies causality and thermodynamic stability leads to the following allowed range for Δ

$$-\frac{2}{3} \leq \Delta \leq \frac{1}{3}. \quad (3)$$

The interest in this quantity stems from the fact that it provides a simple measure of the deviation from conformal symmetry for matter at nuclear and super-nuclear densities. We recall that in QCD the coupling runs with energy, which introduces a scale that breaks conformal symmetry at finite densities and/or temperature. Only at asymptotically large temperatures and/or densities, conformal symmetry is restored and $\Delta = 0$. At finite densities, however, both the value and the sign of the conformal anomaly are not known, although a conjecture was put forth that $\Delta \geq 0$ in neutron-star interiors ([Fujimoto et al. 2022](#)). Here, we test this conjecture and show that besides depending on the lower bound imposed on the maximum mass, the conformal anomaly can vary significantly both in size and sign.

Finally, improved mass measurements of pulsars also induce constraints on the properties of binary neutron-star systems, that can be tested with gravitational-wave detections. For example, the first ever detected gravitational-wave signal of a binary neutron-star merger, i.e., GW170817, set an upper bound on the binary tidal deformability parameter $\tilde{\Lambda} \leq 720$ ([The LIGO Scientific Collaboration et al. 2019](#)), while subsequent early studies have further restricted such uncertainty (see, e.g., [Radice et al. 2018](#); [Most et al. 2018](#)). Using the less conservative maximum-mass bounds of $M_{\text{TOV}} \gtrsim 2.0 M_\odot$, [Altiparmak et al. \(2022\)](#) have recently proposed a simple analytic expression to determine the upper and lower bounds of the tidal deformability in terms of the chirp mass of the binary, i.e., $\tilde{\Lambda}_{\text{min/max}}(M_{\text{chirp}})$. We here reconsider these expressions in the light of the more extreme bounds set by the mass measurement in PSR J0952-0607 and show that for any value of M_{chirp} , only $\tilde{\Lambda}_{\text{min}}$ depends on the assumed maximum mass, while $\tilde{\Lambda}_{\text{max}}$ remains essentially unchanged with respect to the expression presented by [Altiparmak et al. \(2022\)](#).

2 METHODS

To construct the EOSs we employ in our analysis, we follow the procedure by [Altiparmak et al. \(2022\)](#) and [Ecker & Rezzolla \(2022\)](#), to which we refer for more details. In essence, for densities below $n = 0.5 n_s$ we use the Baym-Pethick-Sutherland (BPS) model ([Baym et al. 1971](#)) and extend it until $n = 1.2 n_s$ with random polytropes bounded by the soft and stiff EOSs of [Hebeler et al. \(2013\)](#). For densities $n > 1.2 n_s$, we use the sound-speed interpolation method introduced by [Annala et al. \(2020\)](#) and impose at $n \gtrsim 40 n_s$ the parametrized next-to-next-to leading order (2NLO) perturbative QCD results of ([Fraga et al. 2014](#)) (see also [Gorda et al. \(2021b,a\)](#) for partial 3NLO improvement and [Komoltsev & Kurkela \(2022\)](#) on how to propagate these constraints down to neutron-star densities); we collectively refer to these as to the “QCD” constraints. Note that in contrast to [Altiparmak et al. \(2022\)](#) and [Ecker & Rezzolla \(2022\)](#), we now also perform separate simulations where we do not impose the QCD constraint so as to check its impact on the results.

We also impose constraints from pulsar measurements and binary neutron-star merger observations, to which we collectively refer as “astro” constraints. In particular, we impose the constraints deriving from the radius measurements by the NICER experiment of J0740+6620 ([Miller et al. 2021](#); [Riley et al. 2021](#)) and of J0030+0451 ([Riley et al. 2019](#); [Miller et al. 2019](#)) by rejecting EOSs with $R < 10.75$ km at $M = 2.0 M_\odot$ and $R < 10.8$ km at $M = 1.1 M_\odot$, respectively (see Fig. 1). In addition, we impose the upper bound on the binary tidal deformability parameter $\tilde{\Lambda} \leq 720$ (low-spin priors) obtained from GW170817 ([The LIGO Scientific Collaboration et al. 2019](#)). Denoting respectively with M_i , R_i , and Λ_i the masses, radii, and tidal deformabilities of the binary components, where $\Lambda_i := \frac{2}{3} k_2 (R_i/M_i)^5$, $i = 1, 2$, and k_2 is the second tidal

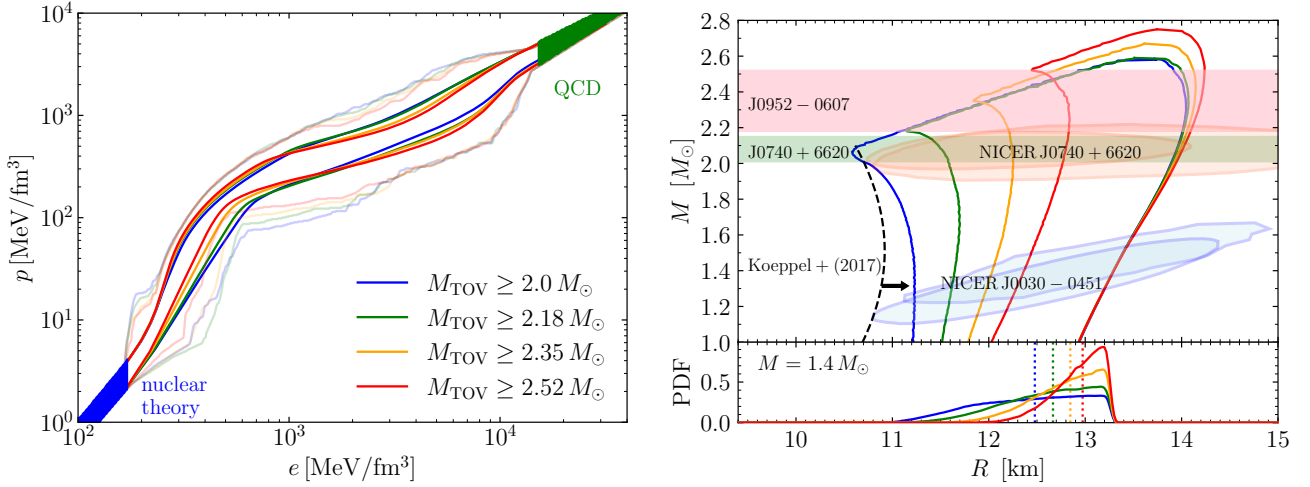


Figure 1. *Left Panel:* PDFs of the various EOSs constructed, with coloured lines showing the 95%-confidence intervals for the different mass constraints. Lines with light colours indicate instead the outer boundaries to excluded regions. The blue and green-shaded areas mark the uncertainty of nuclear theory and perturbative QCD, respectively. *Right Panel:* The same as in the left panel but for the PDFs of the mass-radius relations. Blue and orange ellipses are radius measurements of J0030+0451 (Riley et al. 2019; Miller et al. 2019) and of J0740+6620 (Miller et al. 2021; Riley et al. 2021) by the NICER experiment, respectively. Green and pink areas are mass measurements of J0740+6620 (Fonseca et al. 2021) and J0952-0607 (Romani et al. 2022), respectively. In the bottom part of the panel is reported slices of the PDF for $M = 1.4 M_{\odot}$, with the medians being marked by vertical dotted lines.

Love number, we compute the binary tidal deformability as

$$\tilde{\Lambda} := \frac{16}{13} \frac{(12M_2 + M_1) M_1^4 \Lambda_1 + (12M_1 + M_2) M_2^4 \Lambda_2}{(M_1 + M_2)^5}. \quad (4)$$

For any choice of $M_{1,2}$ and $R_{1,2}$, we then reject those EOSs with $\tilde{\Lambda} > 720$ for a chirp mass $M_{\text{chirp}} := (M_1 M_2)^{3/5} (M_1 + M_2)^{-1/5} = 1.186 M_{\odot}$ and $q := M_2/M_1 > 0.73$ as required for consistency with LIGO/Virgo data for GW170817 (The LIGO Scientific Collaboration et al. 2019).

Because the limits on the maximum mass are still rather uncertain, we perform separate simulations imposing different lower limits on the maximum mass, namely, we consider $M_{\text{TOV}} \geq 2.0, 2.18, 2.35, 2.52 M_{\odot}$, where the first value is motivated by the pulsars PSR J0348+0432 (Antoniadis et al. 2013) ($M = 2.01 \pm 0.04 M_{\odot}$) and PSR J0740+6620 (Cromartie et al. 2019; Fonseca et al. 2021) ($2.08 \pm 0.07 M_{\odot}$), while the last three values correspond to the lower bound, the median and the upper bound of the uncertainty in the mass estimate reported by Romani et al. (2022) for PSR J0952-0607 ($2.35 \pm 0.17 M_{\odot}$). Note that Romani et al. (2022) also reports a more conservative estimate of $M_{\text{TOV}} > 2.09 M_{\odot}$, which we also checked; however because the results are almost indistinguishable from the case $M_{\text{TOV}} \geq 2.0 M_{\odot}$, we do not discuss them here. For each mass-bound considered, we have constructed $\approx 10^6$ different neutron star solutions passing all the QCD and astro constraints.

We remark that in our approach a certain bias inherited from the way the prior is constructed is unavoidable. In our previous works (Altıparmak et al. 2022; Ecker & Rezzolla 2022) we first sampled a temporary maximum value for the maximally allowed sound speed $c_{s,\text{max}}^2$ uniformly in the interval $[0, 1]$ and then the various sound-speed values at the individual matching points for the construction of the EOS on the range $[0, c_{s,\text{max}}^2]$. This approach guaranteed a sufficient sampling rate for globally monotonic and sub-conformal EOS families, which otherwise would be statistically suppressed. Because here we are not interested in such particular subsets of EOSs, we can omit the first step and simply sample the individual sound-speed values between zero and one directly. This approach results in

slightly higher estimates for the sound speed maxima and also slightly different estimates for neutron-star radii compared to our previous work. The resulting difference for the neutrons star radii $R_{1.4(2.0)}$ is negligible, being less than 40(200) m, however, larger differences can appear in the PDF of the maximum sound-speed. One way to mitigate this intrinsic and inevitable bias introduced by the choice of sampling is to employ a Bayesian analysis. A comparison work between our approach and a fully Bayesian approach is presently in progress and will be presented in an upcoming work (Jiang et al. 2022).

Before turning to the results, an important remark is worth making. With a spin frequency of $f = 706$ Hz (Romani et al. 2022) PSR J0952-0607 is the second-fastest-spinning pulsar known. This raises the question of whether the static approximation assumed in our analysis is actually justified and if it is not instead necessary to introduce rotation-induced corrections. To address this question it is sufficient to consider the approximate but analytic quasi-universal expression for the critical mass along the dynamical stability line to gravitational collapse, that is, the value of the maximum mass of a uniformly rotating star when expressed as a function of the dimensionless angular momentum $j := J/M^2$ (Breu & Rezzolla 2016)

$$\frac{M_{\text{crit}}}{M_{\text{TOV}}} = 1 + a_2 \left(\frac{j}{j_{\text{Kep}}} \right)^2 + a_4 \left(\frac{j}{j_{\text{Kep}}} \right)^4, \quad (5)$$

where j_{Kep} is the Keplerian dimensionless angular momentum ($j/j_{\text{Kep}} \leq 1$) and the coefficients have values $a_2 = 0.1316$, $a_4 = 0.07111$. Assuming a Keplerian frequency for PSR J0952-0607 of $f_{\text{Kep}} \approx 1.5$ kHz (see Table 1 of Demircik et al. (2021b)) and expression (5), it is possible to deduce that, in the case of PSR J0952-0607, $f/f_{\text{Kep}} \approx j/j_{\text{Kep}} \lesssim 0.46$, so that the corresponding increase in the maximum mass is less than $0.1 M_{\odot}$, or, equivalently, less than 4% (see also Fig. 4 of Demircik et al. 2021b). In other words, given the much larger uncertainties affecting the maximum mass, the use of the static approximation is well justified and has no relevant impact on our results.

3 RESULTS

We first show in the left panel of Fig. 1 the 95%-confidence intervals (coloured lines) for the EOSs assuming different maximum-mass bounds, together with the corresponding outer envelopes (light coloured lines), where the blue and green shaded areas mark theoretical uncertainties of nuclear theory and perturbative QCD, respectively. Note how larger values for the bound on M_{TOV} lead to a steeper increase of the pressure at energy densities below $e \approx 1 \text{ GeV/fm}^3$. This clearly is a consequence of the increased stiffness necessary to satisfy the larger bounds on M_{TOV} at low densities. The effect is most prominent in the range $0.5 - 1 \text{ GeV/fm}^3$ and pushes the lower 95% contour of the pressure to significantly larger values, while leaving the upper contour almost unchanged. Thus, a simple and interesting result follows from this analysis: large values of M_{TOV} tightly constrain the pressure to be $p \approx 200 \text{ MeV/fm}^3$ at $e \approx 600 \text{ MeV/fm}^3$. On the other hand, in the range $e \approx 1 - 10 \text{ GeV/fm}^3$ the increased mass constraint has the opposite effect: larger bounds on M_{TOV} force the pressure to rise less rapidly. Interestingly, in the intermediate region, (i.e., at $e \approx 1 \text{ GeV/fm}^3$), the bound on M_{TOV} has almost no impact and the EOSs are entirely insensitive to the mass constraints.

In the right panel of Fig. 1 we show instead the 95%-confidence intervals of the mass-radius relations for different maximum-mass bounds (coloured lines). Clearly, large-mass constraints lead to a significant exclusion of stars with small radii, while the upper limit at large radii ($R \approx 13 - 14 \text{ km}$) remains unaffected. The systematic shift towards stellar models with larger radii is clearly a consequence of the stiffening of the EOSs at $e \lesssim 1 \text{ GeV/fm}^3$ shown in the left panel; without this additional pressure support, it is not possible to construct equilibrium models with such large maximum masses. In turn, this means that causality and QCD together with the constraint $M_{\text{TOV}} \gtrsim 2.18 M_\odot$, completely dominate the lower bounds for the stellar radii, rendering the existing radius measurements by the NICER experiments – and which only provide lower limits for the radii – essentially ineffective. The bottom part of the right panel of Fig. 1 reports with coloured lines slices of the probability density functions (PDF) and the corresponding median estimates (dotted lines) for the radii of a typical neutron star with a mass of $M = 1.4 M_\odot$ (see also Table A1 in Appendix A). Larger values for M_{TOV} result in PDFs with significantly smaller probability at small radii, while the sharp edge at large radii set by the tidal deformability constraint remains essentially unaffected. As a result, the median values are shifted to larger values and the uncertainties become smaller, which can be seen more explicitly from the numbers provided in Table A1 of Appendix A.

Figure 2 is used to highlight the impact that a larger mass bound has on the behaviour of the binary tidal deformability. In particular, the figure shows the upper and lower bounds for $\tilde{\Lambda}$ as function of the chirp mass $\mathcal{M}_{\text{chirp}}$. Such bounds were first presented by Altiparmak et al. (2022), where they were shown to follow the simple relation

$$\tilde{\Lambda}_{\text{min(max)}} = a + b \mathcal{M}_{\text{chirp}}^c. \quad (6)$$

This is a particularly important result, since it provides theoretical predictions for the upper and lower bounds on $\tilde{\Lambda}$, a quantity that constrains the EOSs, from $\mathcal{M}_{\text{chirp}}$, a quantity that can be (and has been) measured to high accuracy from the inspiral waveform of binary neutron-star merger events. The colored lines in Fig. 2 show that larger bounds on the maximum mass push $\tilde{\Lambda}_{\text{min}}$ to higher values [the coefficients a, b, c used in Eq. (6) are listed in Table 1], while the upper bound of Altiparmak et al. (2022) remains unaffected: $\tilde{\Lambda}_{\text{max}} = -20 + 1800 \mathcal{M}_{\text{chirp}}^5$. The bottom part of Fig. 2 shows again PDF slices for the chirp mass of GW170817, which has been measured

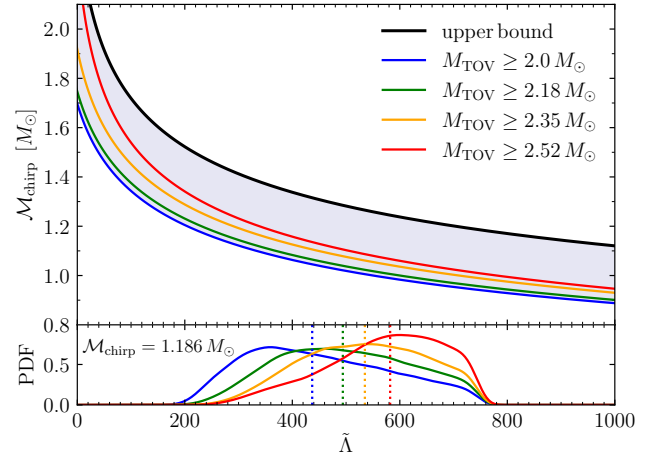


Figure 2. Relation between the chirp mass and binary tidal deformability. Coloured lines mark lower bounds of the 95%-confidence intervals for $\tilde{\Lambda}_{\text{min}}$, while the black line is the upper bound $\tilde{\Lambda}_{\text{max}}$, which is valid for all mass constraints. In the bottom part of the panel are reported the PDF slices for the measured chirp mass of GW170817 $\mathcal{M}_{\text{chirp}} = 1.186 M_\odot$, while the medians are again marked with vertical dotted lines.

Table 1. Best-fit coefficients a, b, c of Eq. (6) for the lower bound of the binary tidal deformability parameter $\tilde{\Lambda}_{\text{min}}$.

$M_{\text{TOV}} [M_\odot]$	a	b	c
≥ 2.00	-50	600	4.7
≥ 2.18	-45	650	4.6
≥ 2.35	-40	750	4.5
≥ 2.52	-20	800	4.4

very accurately to be $\mathcal{M}_{\text{chirp}} = 1.188^{+0.004}_{-0.002}$. Combining the lower limits from all the mass bounds allows us to set the following range for the lower bound on the binary tidal deformability of GW170817 to be $\tilde{\Lambda}_{1.186}^{\text{min}} \in [236, 301]$ for $M_{\text{TOV}} \in [2.18, 2.52] M_\odot$.

We next move on to assessing how the new high-mass bounds on M_{TOV} affect the properties of the spatial distribution of the sound speed in the stellar interior. We do this following a recent work of ours (Ecker & Rezzolla 2022), where we have introduced a novel, scale-independent description of the sound speed in neutron stars where the latter is expressed in a unit-cube spanning the normalised radius, r/R , and the mass normalized to the maximum one, M/M_{TOV} . As shown by Ecker & Rezzolla (2022), a number of interesting results can be deduced from this generic representation. In particular, the top-row of panels in Fig. 3 shows the normalized radial dependence of the sound speed for $M_{\text{TOV}} \geq 2.0 - 2.52 M_\odot$ (left to right). Blue and green-shaded areas denote the 95%-confidence intervals for typical ($M = 1.4 M_\odot$) and maximally massive ($M = M_{\text{TOV}}$) stars, respectively, where the red lines are instead used to mark the median values (see Table A1 in Appendix A).

The finding by Ecker & Rezzolla (2022), that light stars have monotonic sound-speed radial profiles and heavy ones feature a local maximum in the outer layers is even more pronounced when imposing larger bounds on M_{TOV} . Indeed, the larger the maximum-mass constraint, the more asymmetric is the radial distribution of the PDFs, pushing the local maxima of the medians to increasingly larger normalized radii. Exploiting this behaviour, we can set bounds on the value and the location of the median value of the sound-speed maximum in the interior of heavy stars

$$c_{s,\text{max}}^2 \in [0.64, 0.77], \quad \text{for } r/R \in [0.62, 0.72]. \quad (7)$$

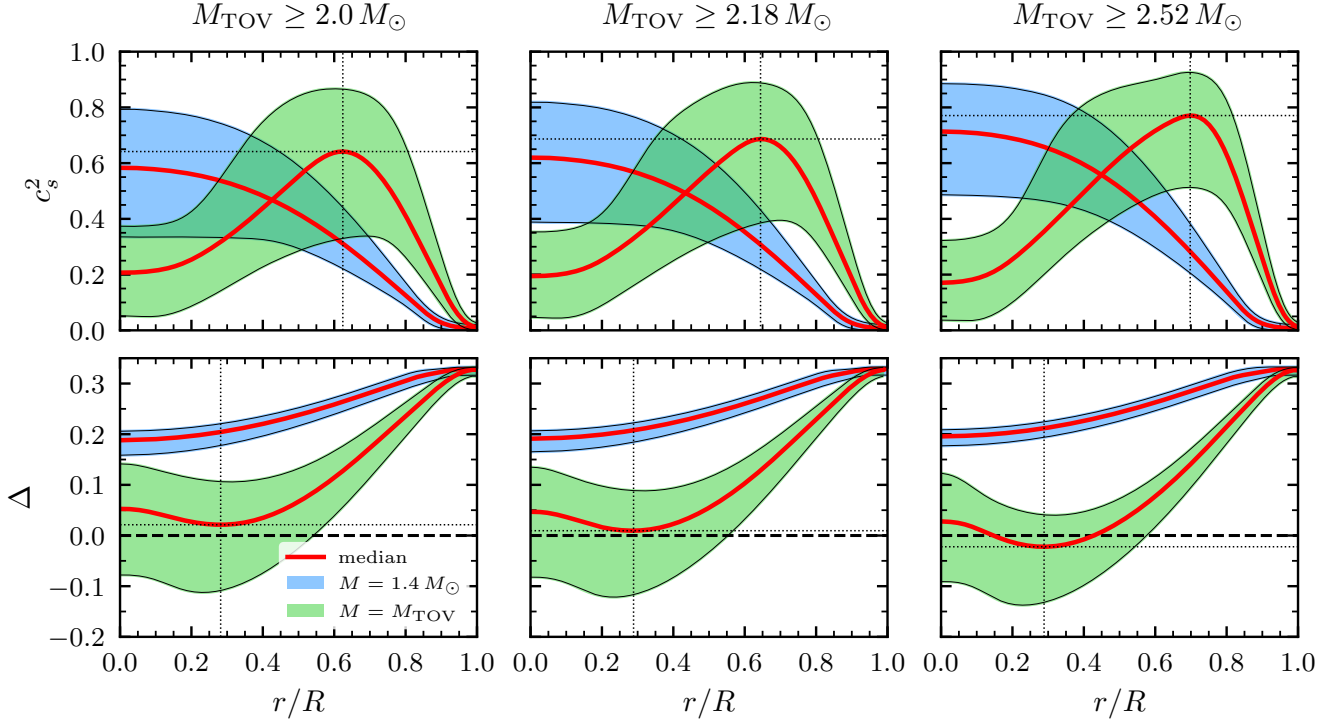


Figure 3. *Top Row:* sound speed as function of normalized radial coordinate r/R inside stars for different values of the mass constraint $M_{\text{TOV}} \geq 2.0 - 2.52 M_{\odot}$ (left to right). Blue and green areas are 95%-confidence intervals for typical ($M = 1.4 M_{\odot}$) and maximally massive ($M = M_{\text{TOV}}$) stars. Dotted black lines indicate the local sound speed maximum in maximally massive stars. *Bottom Row:* The same as in the top row but for the conformal anomaly. Black dashed lines mark $\Delta = 0$, while black dotted lines indicate the local minimum of the conformal anomaly.

Clearly, for larger bounds on M_{TOV} the peak in the sound speed develops already in lighter stars. For the strictest bound, i.e., $M_{\text{TOV}} \geq 2.52 M_{\odot}$, this happens already in stars as light as $\approx 0.6 M_{\text{TOV}}$, whereas for $M_{\text{TOV}} \geq 2.0 M_{\odot}$ the peak appears only at $\approx 0.7 M_{\text{TOV}}$. It is important to recall that the relevance of these results – and their practical application – is that they can be included in nuclear-theory calculations of modern EOSs to constrain the behaviour of the sound speed in those regions where nuclear-theory predictions have large uncertainties.

The bottom-row of Fig. 3 shows instead for the first time the radial dependence of the conformal anomaly Δ given by Eq. (2). Note how, in analogy with what happens for the sound speed, stricter maximum-mass constraints lead to narrower confidence intervals. Towards the stellar surface ($r/R = 1$) the anomaly approaches its vacuum value from below $\Delta \rightarrow 1/3$ independently of the maximum-mass constraint, while the value of Δ in the stellar center ($r/R = 0$) does depend on M_{TOV} . Note that in typical neutron stars with masses $M \sim 1.4 M_{\odot}$, the anomaly decreases monotonically from the surface ($\Delta = 0$) towards the center, where it reaches a median value of $\Delta \approx 0.2$. In turn, this implies $\Delta \geq 0$ inside such stars and that conformal symmetry is broken everywhere in their interior. As shown in Fig. 3, the behaviour of the conformal anomaly in light stars is very robust and depends only very weakly on the different bounds set for the maximum mass (blue-shaded regions). This behaviour, however, ceases to be true for maximally massive stars (green-shaded regions) where the 95%-confidence variance is far larger and where the conformal anomaly exhibits a local minimum $\Delta_{\min} \approx 0$ at $r/R \approx 0.3$. Furthermore, depending on the constraint on M_{TOV} the median value of Δ (red lines) can either be positive or negative (or both) in the

innermost regions of the star. More specifically, for $M_{\text{TOV}} \geq 2.0 M_{\odot}$ we find $\Delta_{\min} > 0$, while for $M_{\text{TOV}} \geq 2.52 M_{\odot}$ the anomaly is $\Delta_{\min} < 0$, somewhat in contrast with the expectations of Fujimoto et al. (2022). In the range $M_{\text{TOV}} \geq 2.18 - 2.35 M_{\odot}$ the value of Δ_{\min} is very close to zero. In other words, depending on the bound set on M_{TOV} , maximally massive stars can either have zero, one, or two layers where conformal symmetry ($\Delta = 0$) is restored.

Finally, we use Fig. 4 to present what is a particularly interesting result: a novel quasi-universal law for the radial distribution of the pressure inside neutrons stars. Adopting the same convention for the shading of the 95%-confidence areas and of the medians of the PDFs, Fig. 4 reports the (normalized) radial dependence of the pressure $p(r/R)/p_c$, where $p_c := p(0)$ is the central pressure. Note how the variance of the $\approx 10^6$ EOSs considered is extremely small both in the case of reference neutron stars with $1.4 M_{\odot}$ (blue-shaded area) and for the maximally massive stars (green-shaded areas), giving a variation from the median value of the median that is $\lesssim 8\%$ (see inset). Also quite remarkable is how the functional behaviour is essentially insensitive to the high-mass bound on M_{TOV} , with differences that are smaller than a few percent even when the largest constraint is imposed on the maximum mass. As a result, this novel relation will likely remain unaffected by more accurate and future maximum-mass measurements and therefore already now represents a robust prediction for the pressure distribution in the interior of neutron stars.

The very tight and quasi-universal behaviour of the pressure profile can be accurately described in terms of a simple fitting formula of

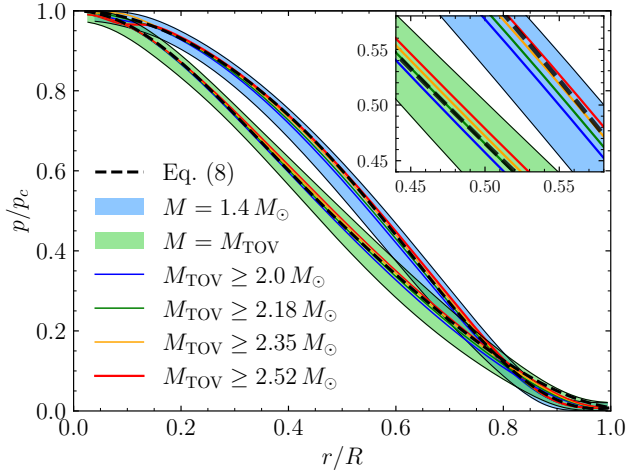


Figure 4. Quasi-universal radial distribution of the pressure in the stellar interior $p(r/R)/p_c$. As in previous figures, blue and green-shaded areas represent the 95%-confidence intervals for typical ($M = 1.4 M_\odot$) and maximally massive ($M = M_{\text{TOV}}$) stars, respectively. Coloured lines are the medians for different lower bounds on M_{TOV} , while the black dashed lines report their best fits using Eq. (8).

the type

$$\frac{p(x)}{p_c} = e^{\alpha x^2} + e^{\alpha \frac{\cos \beta x - 1}{\cos \beta - 1}}, \quad (8)$$

with $x := r/R$ and where the coefficients for maximally massive stars (or for typical $1.4 M_\odot$ stars) are given by $\alpha = 6$ (6.5), $\beta = -5.5$ (−5.5), respectively. Since expression (8) refers to EOSs that by construction satisfy all of the astronomical and QCD constraints, it can be used as a “sanity-check” in the construction of EOSs that start instead from basic principles of theoretical nuclear physics.

4 CONCLUSION

Motivated by the recently announced measurement by [Romani et al. \(2022\)](#) of the neutron-star mass in PSR J0952-0607 with $M = 2.35 \pm 0.17 M_\odot$, we have studied the impact that large bounds on the maximum mass have on the EOS of nuclear matter and on neutron-star properties. To this scope, we have employed an agnostic approach for the construction of EOSs based on a sound-speed parameterisation and that we have carefully tested and exploited in previous works ([Altıparmak et al. 2022](#); [Ecker & Rezzolla 2022](#)).

In this way, we have found that increasingly large bounds on the maximum mass M_{TOV} do change the statistical properties of the EOSs and the corresponding neutron-star characteristics. In particular, the largest bound on the maximum mass coming from PSR J0952-0607 decreases the EOS uncertainty at neutron-star densities significantly, squeezing the 95%-confidence interval for the pressure’s PDF to a narrow band around $p \approx 200 \text{ MeV/fm}^3$ at energy densities $e \approx 600 \text{ MeV/fm}^3$. Furthermore, raising the maximum-mass bound from $2.0 M_\odot$ to $2.52 M_\odot$ increases systematically the radius of a typical neutron star with $1.4 M_\odot$, taking it from a median value $R_{1.4} = 12.48^{+0.75}_{-1.14} \text{ km}$ over to $R_{1.4} = 12.97^{+0.28}_{-0.64} \text{ km}$, reducing at the same time the 95%-confidence level by almost 50%. This behaviour is rather natural and reflects the fact that larger maximum masses require stiffer EOSs and, in turn, stellar models that have on average larger radii. This effect is even more pronounced in the most massive stars, where we find an increase in radius by almost

one kilometre for a reference star with a mass of $2.0 M_\odot$. Because the measurements of the NICER experiment can be used to set lower bounds on the stellar radii, having very large maximum masses has the drawback of making NICER’s constraints largely ineffective.

Another important quantity in our analysis is the (analytic) relation between the binary tidal deformability and the chirp mass $\tilde{\Lambda}(M_{\text{chirp}})$, which has the potential of relating directly a quantity measured with great precision in gravitational-wave detections M_{chirp} with a sensitive property of the EOS $\tilde{\Lambda}$. We have therefore explored what is the impact that larger bounds on the maximum mass have on the resulting relations and found that while the upper bound $\tilde{\Lambda}_{\text{max}}$ is essentially insensitive to changes on M_{TOV} , the lower bound $\tilde{\Lambda}_{\text{min}}$ increases systematically with larger bounds.

Our analysis has also allowed us to explore the scale-independent radial behaviour of the sound speed and, for the first time, of the conformal anomaly Δ within the stellar interior. In this way, we have found that increasing the mass bound from $2.0 M_\odot$ to $2.52 M_\odot$ pushes the maximum sound speed in maximally massive stars from $c_{s,\text{max}}^2 \approx 0.64$ up to $c_{s,\text{max}}^2 \approx 0.77$ and further away from the neutron-star center, i.e., from $r/R \approx 0.62$ to $r/R \approx 0.72$.

We also presented the first results for the radial dependence of the conformal anomaly Δ in the neutron-star interior inspired by the question formulated by ([Fujimoto et al. 2022](#)) on whether Δ is positive definite. Our findings indicate that indeed $\Delta > 0$ in the interior of typical stars with masses of $1.4 M_\odot$, for which Δ decreases monotonically from its vacuum value $\Delta = 1/3$ at the stellar surface down to $\Delta \approx 0.2$ at the neutron-star center. However, for maximally massive stars, the conformal anomaly exhibits a nonmonotonic behaviour inside the star and we show that the value of the anomaly at the local minimum can be either positive, zero or negative, depending on the value for lower bound on M_{TOV} .

Finally, we have reported a novel quasi-universal law for the radial distribution of the pressure inside neutrons stars when cast into a scale-independent manner. The variance around the median is surprisingly small ($\lesssim 8\%$) and the functional behaviour is essentially insensitive to the high-mass bound on M_{TOV} , with differences that are smaller than a few percent even when the largest constraint is imposed on the maximum mass. As a result, this relation will likely remain unaffected by more accurate future maximum-mass measurements and can be used as a “sanity-check” in the theoretical construction of EOSs.

There exists a number of possibilities to generalize our work. One such possibility is to explicitly include first and/or second order phase transitions in the EOS construction. While our method in principle includes such EOSs, they are statistically underrepresented in our ensemble, rendering their impact negligible on the final result. It would also be interesting to test the universal relation for the pressure profile presented in this work in other gravity theories than General Relativity. Finally, another interesting possibility would be to generalize our statistic analysis to rapidly spinning stars, which is numerically more demanding, but feasible and we plan to perform such simulations in future work.

ACKNOWLEDGEMENTS

We thank T. Gorda and A. Kurkela for useful discussions. Partial funding comes from the State of Hesse within the Research Cluster ELEMENTS (Project ID 500/10.006), by the ERC Advanced Grant “JETSET: Launching, propagation and emission of relativistic jets from binary mergers and across mass scales” (Grant No. 884631). CE acknowledges support by the Deutsche Forschungsgemeinschaft

(DFG, German Research Foundation) through the CRC-TR 211 “Strong-interaction matter under extreme conditions” – project number 315477589 – TRR 211. LR acknowledges the Walter Greiner Gesellschaft zur Förderung der physikalischen Grundlagenforschung e.V. through the Carl W. Fueck Laureatus Chair. The calculations were performed on the local ITP Supercomputing Clusters Iboga and Calea.

DATA AVAILABILITY

Data is available upon reasonable request from the corresponding author.

REFERENCES

- Altirparmak S., Ecker C., Rezzolla L., 2022, arXiv e-prints, [p. arXiv:2203.14974](#)
- Annala E., Gorda T., Kurkela A., Nättilä J., Vuorinen A., 2020, *Nature Physics*, **16**, 907
- Antoniadis J., et al., 2013, *Science*, **340**, 6131
- Baiotti L., Rezzolla L., 2017, *Rept. Prog. Phys.*, **80**, 096901
- Bastian N.-U. F., 2021, *Phys. Rev. D*, **103**, 023001
- Baym G., Pethick C., Sutherland P., 1971, *Astrophys. J.*, **170**, 299
- Bedaque P., Steiner A. W., 2015, *Physical Review Letters*, **114**, 031103
- Bozzola G., Espino P. L., Lewin C. D., Paschalidis V., 2019, *European Physical Journal A*, **55**, 149
- Brandes L., Weise W., Kaiser N., 2022, arXiv e-prints, [p. arXiv:2208.03026](#)
- Braun J., Schallmo B., 2022, arXiv e-prints, [p. arXiv:2204.00358](#)
- Breu C., Rezzolla L., 2016, *Mon. Not. R. Astron. Soc.*, **459**, 646
- Cromartie H. T., et al., 2019, *Nature Astron.*, **4**, 72
- Demircik T., Ecker C., Järvinen M., 2021a, arXiv e-prints, [p. arXiv:2112.12157](#)
- Demircik T., Ecker C., Järvinen M., 2021b, *Astrophys. J. Lett.*, **907**, L37
- Dietrich T., Coughlin M. W., Pang P. T. H., Bulla M., Heinzl J., Issa L., Tews I., Antier S., 2020, *Science*, **370**, 1450
- Drischler C., Melendez J. A., Furnstahl R. J., Phillips D. R., 2020, *Phys. Rev. C*, **102**, 054315
- Duarte D. C., Hernandez-Ortiz S., Jeong K. S., McLerran L. D., 2021, *Phys. Rev. D*, **104**, L091901
- Ecker C., Rezzolla L., 2022, arXiv e-prints, [p. arXiv:2207.04417](#)
- Ecker C., Hoyos C., Jokela N., Rodríguez Fernández D., Vuorinen A., 2017, *JHEP*, **11**, 031
- Fonseca E., et al., 2021, *Astrophys. J. Lett.*, **915**, L12
- Fraga E. S., Kurkela A., Vuorinen A., 2014, *Astrophys. J. Lett.*, **781**, L25
- Freedman B. A., McLerran L. D., 1977, *Phys. Rev. D*, **16**, 1169
- Fujimoto Y., Fukushima K., McLerran L. D., Praszalowicz M., 2022, arXiv e-prints, [p. arXiv:2207.06753](#)
- Gandolfi S., Lippuner J., Steiner A. W., Tews I., Du X., Al-Mamun M., 2019, arXiv e-prints, [p. arXiv:1903.06730](#)
- Gorda T., Kurkela A., Paatelainen R., Säppi S., Vuorinen A., 2021a, *Phys. Rev. D*, **104**, 074015
- Gorda T., Kurkela A., Paatelainen R., Säppi S., Vuorinen A., 2021b, *Phys. Rev. Lett.*, **127**, 162003
- Gorda T., Komoltsev O., Kurkela A., 2022, arXiv e-prints, [p. arXiv:2204.11877](#)
- Greif S. K., Raaijmakers G., Hebeler K., Schwenk A., Watts A. L., 2019, *Mon. Not. R. Astron. Soc.*, **485**, 5363
- Hebeler K., Lattimer J. M., Pethick C. J., Schwenk A., 2013, *Astrophys. J.*, **773**, 11
- Hoyos C., Jokela N., Rodríguez Fernández D., Vuorinen A., 2016, *Phys. Rev. D*, **94**, 106008
- Ivanytskyi O., Blaschke D., 2022, *Eur. Phys. J. A*, **58**, 152
- Jiang J.-L., Ecker C., Rezzolla L., in preparation, 2022, arXiv e-prints
- Kanakis-Pegios A., Koliogiannis P. S., Moustakidis C. C., 2020, *Phys. Rev. C*, **102**, 055801
- Keller J., Wellenhofer C., Hebeler K., Schwenk A., 2021, *Phys. Rev. C*, **103**, 055806
- Komoltsev O., Kurkela A., 2022, *Phys. Rev. Lett.*, **128**, 202701
- Leonhardt M., Pospiech M., Schallmo B., Braun J., Drischler C., Hebeler K., Schwenk A., 2020, *Phys. Rev. Lett.*, **125**, 142502
- Marczenko M., McLerran L., Redlich K., Sasaki C., 2022, arXiv e-prints, [p. arXiv:2207.13059](#)
- Margalit B., Metzger B. D., 2017, *Astrophys. J. Lett.*, **850**, L19
- Margueron J., Hansen H., Proust P., Chanfray G., 2021, *Phys. Rev. C*, **104**, 055803
- McLerran L., Reddy S., 2019, *Phys. Rev. Lett.*, **122**, 122701
- Miller M. C., et al., 2019, *Astrophys. J. Lett.*, **887**, L24
- Miller M. C., et al., 2021, *Astrophys. J. Lett.*, **918**, L28
- Most E. R., Weih L. R., Rezzolla L., Schaffner-Bielich J., 2018, *Phys. Rev. Lett.*, **120**, 261103
- Moustakidis C. C., Gaitanos T., Margaritis C., Lalazissis G. A., 2017, *Physical Review C*, **95**, 045801
- Nathanail A., Most E. R., Rezzolla L., 2021, *ApJ*, **908**, L28
- Pal S., Kadam G., Bhattacharyya A., 2022, *Nucl. Phys. A*, **1023**, 122464
- Radice D., Perego A., Zappa F., Bernuzzi S., 2018, *Astrophys. J. Lett.*, **852**, L29
- Rezzolla L., Zanotti O., 2013, *Relativistic Hydrodynamics*. Oxford University Press, Oxford, UK, [doi:10.1093/acprof:oso/9780198528906.001.0001](#)
- Rezzolla L., Most E. R., Weih L. R., 2018, *Astrophys. J. Lett.*, **852**, L25
- Riley T. E., et al., 2019, *Astrophys. J. Lett.*, **887**, L21
- Riley T. E., et al., 2021, *Astrophys. J. Lett.*, **918**, L27
- Romani R. W., Kandel D., Filippenko A. V., Brink T. G., Zheng W., 2022, *Astrophys. J. Lett.*, **934**, L18
- Ruiz M., Shapiro S. L., Tsokaros A., 2018, *Phys. Rev. D*, **97**, 021501
- Shao L., Yagi K., 2022
- Shibata M., Zhou E., Kiuchi K., Fujibayashi S., 2019, *Phys. Rev. D*, **100**, 023015
- Somasundaram R., Tews I., Margueron J., 2022, arXiv e-prints, [p. arXiv:2204.14039](#)
- The LIGO Scientific Collaboration et al., 2019, *Physical Review X*, **9**, 011001
- Vuorinen A., 2003, *Phys. Rev. D*, **68**, 054017
- Yagi K., Yunes N., 2013, *Science*, **341**, 365

APPENDIX A: IMPACT OF QCD CONSTRAINTS

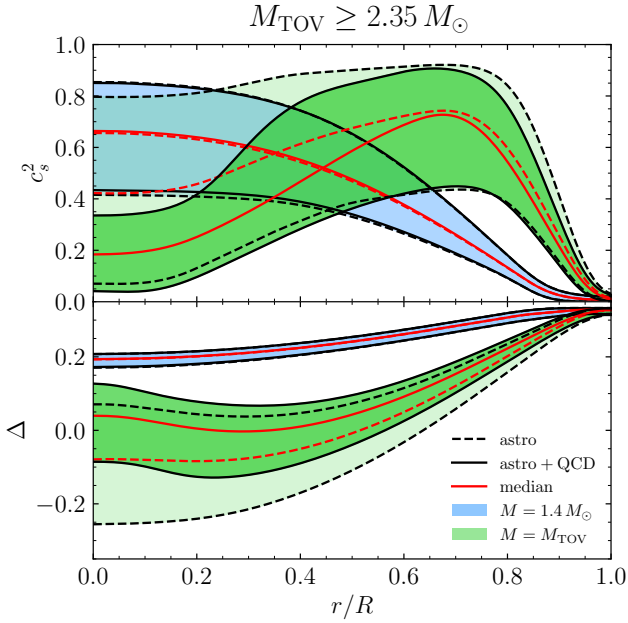
We first collect in Table A1 the numerical values of the various EOSs and neutron-star properties discussed in the main text. We list results for cases where we impose constraints that are only “astro”, or only “QCD”, or their combination “astro+QCD”. The QCD constraints have the largest impact on the minimum values of the conformal anomaly Δ_{\min} and the sound speed in the neutron star center $c_{s,\text{center}}^2$. Note that there is a clear trend, namely that Δ_{\min} is systematically underestimated, while $c_{s,\text{center}}^2$ is systematically over estimated if QCD is not imposed.

Next, we consider how perturbative QCD boundary conditions imposed in model-agnostic approaches can have a relevant impact on the EOSs at densities realised in neutron stars close to their maximum mass (Somasundaram et al. 2022; Gorda et al. 2022). We study the impact of these boundary conditions by comparing results where they are imposed to those where they are not imposed. While the impact on our estimated for neutron-star radii is rather small, the relative differences of the conformal anomaly and the sound speed inside maximally massive stars can be significant, which allows us to identify these quantities as particular sensitive to the perturbative QCD boundary conditions. In Figure A1 we exemplify the impact of QCD constraints on the sound-speed distribution and the conformal anomaly inside stars for the case $M_{\text{TOV}} \geq 2.35 M_{\odot}$.

We find the impact of QCD on typical stars is negligible, but this is entirely different in maximally massive stars. There the quantitative

Table A1. Impact of constraints on neutron-star properties. Taking as a reference maximally massive stars of mass $M = M_{\text{TOV}}$, the various columns report: the minimum values of the conformal anomaly Δ_{min} , the sound speed at the neutron-star center $c_{s,\text{center}}^2$, the maximum sound speed $c_{s,\text{max}}^2$ and its radial location inside stars r_{max}/R . Also listed are the radii $R_{1.4}$ ($R_{2.0}$) of stars with mass $M = 1.4$ (2.0) M_{\odot} , the binary tidal deformability $\tilde{\Lambda}_{1.186}$ of a GW170817-like event and the minimum compactness $C_{\text{TOV}}^{\text{min}}$ of maximally massive stars. Quantities with error estimates correspond to median values and uncertainties to 95%-confidence intervals. Note that are reported values in which either the “astro” or the “QCD” or both constraints “astro+QCD” are imposed.

M_{TOV}/M_{\odot}	Constraints	Δ_{min}	$c_{s,\text{center}}^2$	$c_{s,\text{max}}^2$	r_{max}/R	$R_{1.4}$ [km]	$R_{2.0}$ [km]	$\tilde{\Lambda}_{1.186}$	$C_{\text{TOV}}^{\text{min}}$
≥ 2.00	astro	$-0.05^{+0.14}_{-0.18}$	$0.38^{+0.40}_{-0.33}$	$0.68^{+0.21}_{-0.34}$	0.63	$12.59^{+0.65}_{-1.23}$	$12.49^{+1.33}_{-1.63}$	415^{+283}_{-178}	0.222
	astro+QCD	$+0.02^{+0.08}_{-0.13}$	$0.21^{+0.17}_{-0.15}$	$0.64^{+0.22}_{-0.31}$	0.62	$12.48^{+0.75}_{-1.14}$	$12.32^{+1.43}_{-1.47}$	412^{+282}_{-176}	0.221
≥ 2.18	astro	$-0.06^{+0.13}_{-0.17}$	$0.39^{+0.38}_{-0.33}$	$0.73^{+0.19}_{-0.34}$	0.65	$12.72^{+0.54}_{-1.13}$	$13.00^{+0.86}_{-1.61}$	434^{+266}_{-180}	0.236
	astro+QCD	$+0.01^{+0.08}_{-0.13}$	$0.19^{+0.16}_{-0.15}$	$0.69^{+0.20}_{-0.30}$	0.64	$12.67^{+0.67}_{-1.05}$	$12.92^{+0.89}_{-1.42}$	449^{+253}_{-183}	0.235
≥ 2.35	astro	$-0.08^{+0.13}_{-0.16}$	$0.42^{+0.37}_{-0.35}$	$0.74^{+0.18}_{-0.31}$	0.68	$12.82^{+0.43}_{-0.92}$	$13.20^{+0.66}_{-1.21}$	524^{+205}_{-223}	0.251
	astro+QCD	$+0.00^{+0.07}_{-0.12}$	$0.18^{+0.15}_{-0.14}$	$0.72^{+0.18}_{-0.28}$	0.68	$12.85^{+0.40}_{-0.83}$	$13.25^{+0.60}_{-1.09}$	485^{+231}_{-191}	0.250
≥ 2.52	astro	$-0.10^{+0.12}_{-0.15}$	$0.44^{+0.38}_{-0.37}$	$0.77^{+0.16}_{-0.28}$	0.70	$12.94^{+0.34}_{-0.76}$	$13.41^{+0.47}_{-0.94}$	498^{+303}_{-215}	0.266
	astro+QCD	$-0.02^{+0.06}_{-0.11}$	$0.17^{+0.15}_{-0.13}$	$0.77^{+0.15}_{-0.26}$	0.70	$12.97^{+0.28}_{-0.64}$	$13.47^{+0.42}_{-0.80}$	517^{+206}_{-216}	0.266
	QCD	$+0.02^{+0.12}_{-0.15}$	$0.25^{+0.30}_{-0.19}$	$0.54^{+0.28}_{-0.31}$	0.55	$11.02^{+3.24}_{-3.20}$	$13.00^{+2.30}_{-2.54}$	285^{+598}_{-256}	–



This paper has been typeset from a \LaTeX file prepared by the author.

Figure A1. The same as in Fig. 3 but when consider the differential impact of the astro (black solid lines) and astro+QCD (black dashed lines) constraints. Red lines mark the median, with solid (dashed) lines including (exclude) the QCD constraints.

and even the qualitative behavior of c_s^2 and Δ in the core is very different. Without imposing QCD, the conformal anomaly decreases monotonically towards the stellar center, where its value is negative. Also the confidence interval gets very wide, which is a sign that without the QCD boundary conditions Δ and c_s^2 are not well constrained in the centres of heavy stars. This can be seen particularly well on c_s^2 , whose confidence interval increases from a quite narrow band $\approx 0 - 0.3$ in the constrained case to $\approx 0 - 0.8$ in the unconstrained case. In consequence, there is 100% difference in the median values of the sound speed $c_{s,\text{center}}^2 = 0.2$ (with QCD) versus 0.4 (without QCD). In summary, QCD has negligible impact on the mass-radius relation, but is important to determine the radial distribution of the sound speed and the conformal anomaly of massive stars.